frontiers | Frontiers in Materials

TYPE Original Research
PUBLISHED 10 January 2023
DOI 10.3389/fmats.2022.1107193

OPEN ACCESS

EDITED BY
Yang Yu,
University of New South Wales, Australia

REVIEWED BY
Shaoqi Li,
Nanjing Tech University, China
Xian-Xu Bai,
Hefei University of Technology, China

*CORRESPONDENCE
Yazhou Wang,
wangyz@bjtkgd.com

SPECIALTY SECTION
This article was submitted to Smart Materials, a section of the journal Frontiers in Materials

RECEIVED 24 November 2022
ACCEPTED 23 December 2022
PUBLISHED 10 January 2023

CITATION
Cui S, Liu B, Zhou Y, Liu C, Wang Y and Xiao J (2023), Development of magnetorheological elastomer railway pads with a tunable stiffness/damping property for railway fastening systems. *Front. Mater.* 9:1107193.
doi: 10.3389/fmats.2022.1107193

Development of magnetorheological elastomer railway pads with a tunable stiffness/damping property for railway fastening systems

Shukun Cui[1,2], Bingtong Liu[1,3], Yao Zhou[3], Changxi Liu[3], Yazhou Wang[1,3]* and Junheng Xiao[1,2,3]

[1]Railway Engineering Research Institute, China Academy of Railway Sciences Group Co., Ltd, Beijing, China, [2]State Key Laboratory of Track Technology for High Speed Railway, Beijing, China, [3]Research Center, Beijing Tiekeshougang Railway Technology Co., Ltd, Beijing, China

The railway pad plays an irreplaceable role in isolating the vibration and noise from rail/wheel interaction in railway components. A railway pad with variable stiffness and damping properties can adapt to various railway operating conditions for suppressing of railway noise and vibration. Unfortunately, to meet the practical requirements in railway fastening systems, which the railway pad should be able to bear heavy loads with low stiffness, both the material development and structural design need to be addressed for the application of magnetorheological elastomer (MRE). In this work, an MRE railway pad is designed, developed and experimentally tested. As illustrated by experimental results, the obtained MRE materials illustrate an obvious magnetorheological effect with the highest efficiency of 171% on storage modulus and 70% on loss factor. Coupling with the magnet controlling unit, the MRE railway pad is capable to control the stiffness and damping property under high loads. By adjusting the coil's current from 0 A to 5 A, its static stiffness exhibits an enhancement from 37.9 kN/mm to 68.4 kN/mm, and the damping property increases from 8776.3 N•s/m to 10866.3 N•s/m. These results in this study are not only a successful demonstration of delivering a tunable stiffness and damping capability of the railway pad, but also pave the way for the development of MRE materials to achieve more rational applications.

KEYWORDS

magnetorheological elastomer, tunable stiffness, damping properties, railway pad, railway fastening systems

1 Introduction

Railway transportation systems are well developed and widely applied to meet high demands from fast growth of population, due to its freight capacity, high efficiency and minimal environmental impact (Ph Papaelias, M., et al., 2008; Gao, X., et al., 2019). A well-known issue in the railway systems, especially in the high-speed railway, is vibration, which causes two distinct effects, wayside noise and track vibration. These negative effects are not only deteriorating the wellbeing of residents living near to railway, but also shortening the life cycle of railway components, such as wheel polygonization and track irregularity. In addition, the increasing train speed and loads causes a higher dynamic force on wheel/rail interactions as well as noise and vibration.

TABLE 1 Composition of MRE railway pad.

Materials	Wt% (phr)
110 Silicone Gum	83
Dihydroxydiphenylsilane	4
CIP	70
Iron oxides	5
Benzoyl peroxide	0.7
Divinyl tetramethyl disiloxane	8

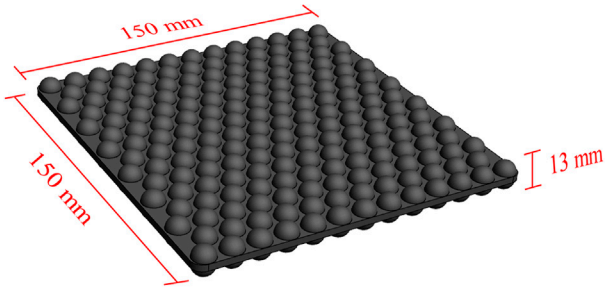

FIGURE 1
The design and structure of MRE railway pad.

It is well known that the structural stiffness beneath the rail is the main factor in noise and vibration (Sol-Sánchez, M., et al., 2015). In common a high-speed slab track system, the low stiffness rail pad is applied to overcome the shock load from wheels to track structures, and therefore to isolate track vibrations response from wheel rolling (Sainz-Aja, J. A., et al., 2020). However, the unreasonably low stiffness may bring the violent wheel/rail interactions when the critical speed is more than 150 km/h, especially in the presence of track irregularity with high amplitude (Khajehdezfuly, A. 2019; Maes, J., et al., 2006). For a traditional railway pad, its stiffness is fixed after structural design and installation, which cannot adapt to the various working conditions, such as different track irregularities, train operation speed and loading weight. Hence, a desirable stiffness of railway pad could be capable of adapting the different track styles, trans weights and damping needs.

A novel material, so called magnetorheological elastomer (MRE), exhibits a unique mechanical property which can change its Young's modulus, natural frequency and damping capacity under the external magnetic field, because of as the magnetorheological (MR) effect (Ahmad Khairi, M. H., et al., 2019; Schubert, G. and Harrison, P. 2015; Li, S., et al., 2020; Yu, Y., et al., 2019). This unique rheological property is due to the presence of ferromagnetic particles in the rubber matrix, in which the suspended particles induce magnetic interaction and stress transfer *via* the external magnetic field (Chen, L., et al., 2007; Makarova, L. A., et al., 2019). The alteration of MRE materials into traditional devices could improve its adapting performance or extend its engineering applications, such as vibration isolators, vibration absorbers, sensing devices, actuators and magnetic pumps (Liu, C., et al., 2020; Yu, Y., et al., 2020). Based on the special feature of MRE materials, whose stiffness and damping properties differ according to the external magnetic field, tunable vibration isolators are developed and demonstrated in many studies (Yu, Y., et al., 2016; Behrooz, M., et al., 2014; Li, W., et al., 2012; Bastola, A. K. and Li, L. 2018). Sun, S. S., et al. (2014) develops an adaptive tuned MRE absorber, whose natural frequency can shit form 37 Hz to 67 Hz working in squeeze mode. This kind of adaptive tuned MRE absorber has more active range than the passive absorber. For large-scale building isolation, a series of laminated MRE isolators are reported with an maximum percentage increase of 38% on the stiffness and damping ratio in the shear deformation (Li, Y., et al., 2013; Li, Y., et al., 2013). The MRE isolator is also designed in shear-compression mixed mode. The small-scale porotypes illustrate a superior changeable capability, of which the natural frequency, stiffness and damping can increase to 103%, 329.63%, and 180.31%, respectively. An MRE rubber train joint is demonstrated by Sun, S., et al. (2017), with MRE materials, this train rubber joint exhibits various stiffness to adapt to the track trafficability and high-speed stability. Umehara and Mitsumata propose a kind of railway actuator with tunable stiffness made of MRE materials, which is mounted between the bogue frame and the axle box of the railway vehicle. When the test vehicle runs at a speed of 15 km/h, the results reveal that the lateral force between the rail and wheel is reduced by 20% under the external magnetic field (Yasuhiro, et al., 2018).

Integration of the MRE materials into the railway fastening system as railway pads is a novel approach to endow its capability of tunable stiffness/damping properties. The MRE prepared with liquid precursors is preferred since soft elastomeric matrixes provide less resistance against particle movement. Although MRE rubbers fabricated with such methods normally shows a higher MR efficiency compared with other types of rubber matrixes, it is restricted for rational applications because of their limited bearing capacity (Shuib, R. K., et al., 2015; Yoon, J.-H., et al., 2022). Therefore, both the material development and structural design are equally essential to develop the MRE railway pads in the railway fastening system, where the loads as high as 55 kN are applied. In this work, an MRE railway pad is proposed and fabricated based on thermal plastic silicone vulcanizate matrix, and then a magnetic controlling unit is designed to adjust the magnetic field. According to working requirements of railway pads, the tunable capabilities on stiffness/damping properties of the MRE railway pad are investigated *via* experimental measurement.

2 Materials and preparation

The components used for the fabrication of the MRE railway pad includes 110 silicone gum, dihydroxy-diphenylsilane, carbonyl iron particles (CIP, CD grade, BASF), Iron oxides, benzoyl peroxide, divinyl tetramethyl disiloxane. The weight concentration of all components is listed in Table 1. There are three steps in fabricating procedures of the MRE railway pad: mixing, magnetic alignment and vulcanization. The 110-silicone gum is firstly put into a Banbury mixer for 2 min at 60°C with a rotation speed of 40 rad/min. Then, the weighted dihydroxydiphenylsilane, CIP and divinyl tetramethyl disiloxane are gently added into a mixer, and mixed for 5 min. The compounded rubber is obtained after another 4 min mixing with the addition of benzoyl peroxide, divinyl tetramethyl disiloxane. The compounded rubber is further mixed by a double roll milling machine at a temperature below 55°C. In the magnetic alignment step, the compounded rubber is compressed into a

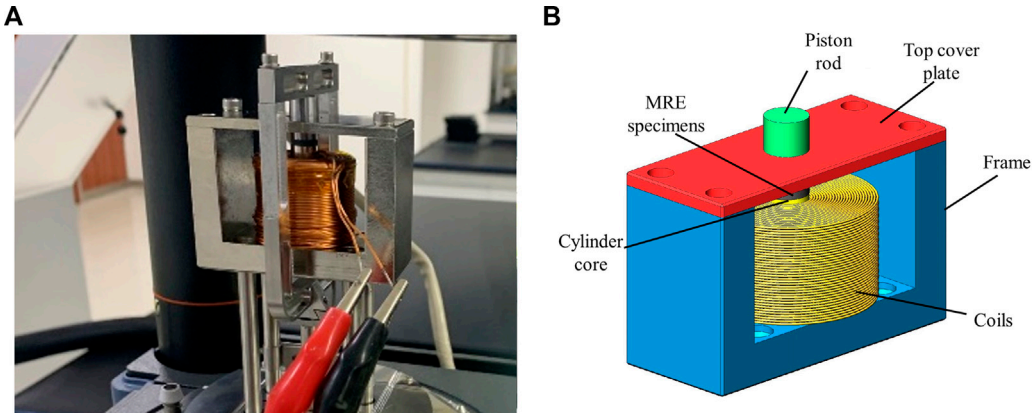

FIGURE 2
DMA measurement **(A)** and clamps **(B)** of MRE materials.

designed mold and then put the whole mold into an external magnetic field to align the CIP along the vertical direction and chain-like structures for 30 min. Finally, the MRE railway pad is obtained by vulcanization of molded rubber with compressive stress of 15 MPa at 160°C for 10 min.

In order to bear the heavy load with low stiffness for the application to the railway fastening system, the structure of MRE railway pad is designed as a double-layer hemispherical bump structure, as shown in Figure 1. The diameter of the hemispheres is 10 mm, the spacing between adjacent hemispheres is 1.8 mm with the diplarthrous arrangement. The thickness of the plate layer is 3mm, the hemispherical bumps are symmetrically arranged on both sides, and the total thickness of the backing plate is 13 mm. The designed structure can fulfil the free deformation on lateral direction by compressive loads.

3 Results and discussion

3.1 Rheological measurement of MRE materials

The rheological properties of the MRE material samples are examined by a commercial dynamic mechanical analysis (DMA) instrument (Q800, T.A. instruments) in compressive mode. When the ideal viscoelastic material is subjected to sine-wave stress, the stress response behavior is nether the ideal elastic solid nor the ideal viscous liquid. In this moment the relationship between stress and strain can be described as:

$$\boldsymbol{\varepsilon = \varepsilon_0 \, sin\,(\omega t)} \tag{1}$$

$$\boldsymbol{\sigma = \sigma_0 \, sin\,(\omega t)\, cos\,(\delta) + \sigma_0 \, cos\,(\omega t)\, sin\,(\delta)} \tag{2}$$

where the ε_0 is strain amplitude, ω is angular frequency and σ_0 is stress amplitude (Moreno, M. A., et al., 2021). By substituting the equation of storage modulus $E_1 = \sigma_0/\varepsilon_0 \cos(\delta)$, loss modulus $E_2 = \sigma_0/\varepsilon_0 \sin(\delta)$, loss factor $\eta = \frac{E_2}{E_1} = \tan(\delta)$, and the Eq. 1 into Eq. 2, the rheological properties of the MRE material can be expressed as follows:

$$\boldsymbol{\sigma = E_1 \varepsilon + E_2 \omega \dot{\varepsilon}} \tag{3}$$

To exert the external magnetic field, a home-made clamp is designed and installed in the DMA instrument, as shown in Figure 2A. This testing clamp is consisted of a magnetic induction frame (low-carbon steel), cylinder core (low-carbon steel), cooper coils (self-adhesive coils), piston rod (low-carbon steel) and top cover plate (low-carbon steel), as illustrated in Figure 2B. In addition, the steel frame is fastened on the DMA base and the piston rod is connected to the aluminum loading bearer. The external magnetic is applied by a DC-regulated power supply and controlled by adjusting the coil current. The MRE specimens are cut into small cylinders with a size of 9 mm diameter and 2 mm height for DMA measurements. The dynamic properties dependent on the frequency of the MRE specimens are investigated under a static load of 2 N and dynamic amplitude of 2 μm from 1 to 100 Hz at room temperature. Frequency dependences of the storage modulus and loss factor are shown in Figure 3, measured at different coil's currents. With the excitation frequency of dynamic load varying from 1 to 100 Hz, the storage modulus has an obvious enhancement. Similarly, a slight increasement from 0.25 to 0.35 in loss factor is observed without any external magnetic field. By introducing the external magnetic field, both storage modulus and loss factor are enhanced for all excitation frequencies, which is due to the MR effects.

Based on the relationship between the storage modulus/loss factor and current in coils, the MR efficiency can be calculated as:

$$\boldsymbol{e_{storage} = \frac{G - G_0}{G_0} \times 100\%} \tag{4}$$

$$\boldsymbol{e_{loss\,factor} = \frac{tan\,\theta' - tan\,\theta}{tan\,\theta} \times 100\%} \tag{5}$$

where $e_{storage}$ and $e_{loss\,factor}$ are the MRE efficiency of storage modulus and loss factor of MRE specimens, respectively; G and G_0 are the storage modulus with external magnetic field and initial storage modulus, respectively; $\tan\theta'$ and $\tan\theta$ are the loss factor with and without external magnetic field, respectively (Gong, X. L., et al., 2007). The relationship between MR efficiency and current is shown in Figure 4. The MR efficiency of storage modulus illustrates a similar trend for all excitation frequencies, and it linearly increases by enhancing the current from 0 to 1.6 A. The maximum MR efficiency of storage modulus reaches 171 % at 100 Hz with 1.6 A. In addition, the MR efficiency of loss factor increases with the growth of external magnetic field. However, in

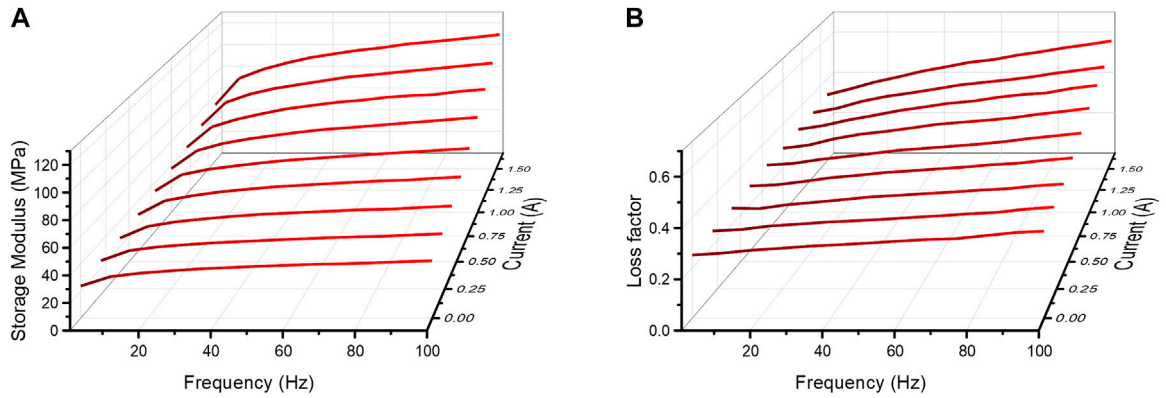

FIGURE 3
Storage modulus **(A)** and loss factor **(B)** of MRE specimens at different current for frequency sweep test.

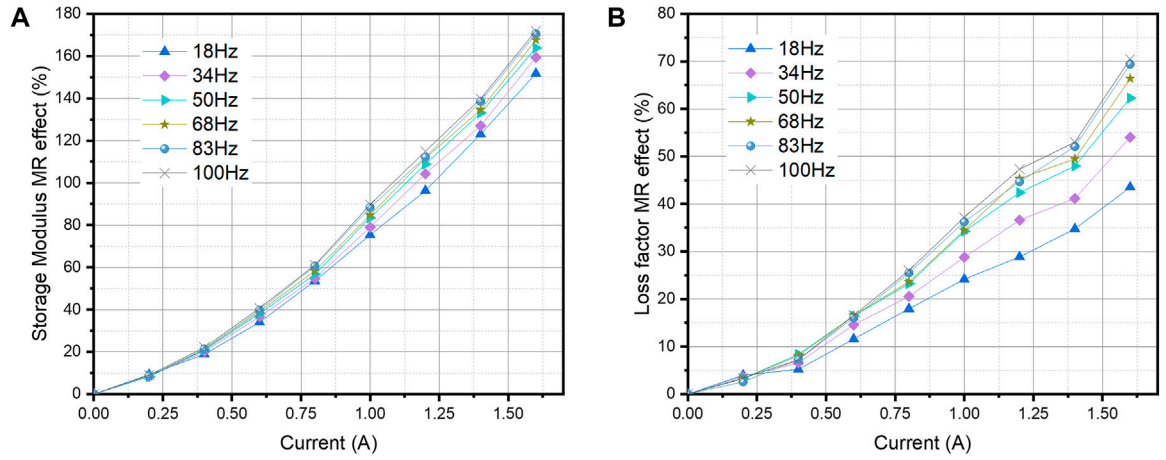

FIGURE 4
MR efficiency of Storage modulus **(A)** and loss factor **(B)** of the MRE specimen at different current.

contrast of storage modulus, the loss factors are dependent on both the frequency and the intensity of the external magnetic field, which it is observed a higher MR efficiency at high frequency range. The maximum MR efficiency of loss factor reaches 70 % at 100 Hz with 1.6 A. The results indicate that the obtained MRE railway pads could change their stiffness and damping properties by meet the demand of magnetic field.

3.2 Structural design of magnetic controlling unit based on MRE railway pad

For all components in track structures, the rail fastening system provides vibration insulation through the railway pad, which is installed between the rail and the sleeper. In this regard, a magnetic controlling unit is designed as shown in Figure 5. This magnetic controlling unit couples an MRE railway pad instead of the traditional railway pad to deliver the capability of tunable stiffness and

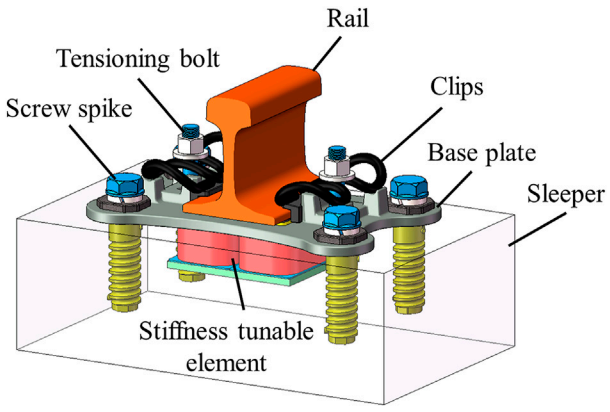

FIGURE 5
Design and structure of railway fastening system with MRE railway pad and magnetic controlling unit.

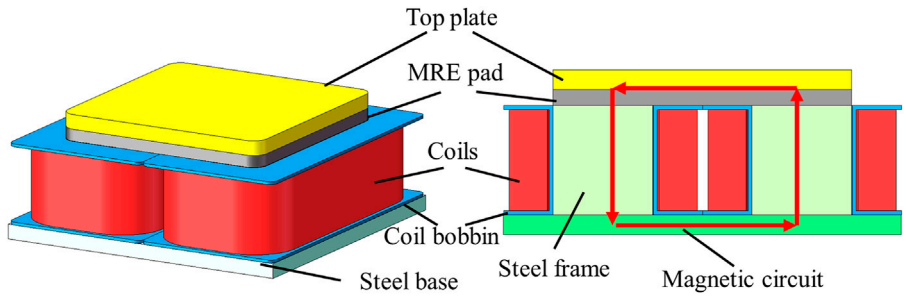

FIGURE 6
Design and structure of magnetic controlling unit coupled with MRE railway pad.

TABLE 2 Structural parameters of magnetic controlling unit.

Structural parameters	Value	Coil parameters	Value
Width of steel frame	50 mm	Number of coil turns	800
Length of steel frame	150 mm	Current	0–5A
Height of steel frame	50 mm	Height of coil	50 mm
Height of steel base	30 mm	Width of coil	23 mm
Height of MRE railway pad	13 mm	Thickness of coil bobbin	2 mm
Height of top plate	30 mm	Air gap	0.5 mm

damping performance as illustrated in Figure 6. Apart from copper coils and aluminum coil bobbin, all parts are made of #10 steel to be rigid under heavy load.

Magnetostatic analysis of the whole device is also carried out to further examine the capability to adjust the required magnetic flux density through the MRE railway pads. For this purpose, the finite element method (FEM) is utilized to analyze the strength and distributions with solid96 elements *via* the commercial software ANSYS. The structural parameters of all parts, including the top plate, steel frame, steel base, MRE railway pad, coils and coil bobbins in the designed device are listed in Table 2. The relative permeability of the MRE railway pad is set to three under the ambient conditions (Fu, J., et al., 2013). The distribution of magnetic flux density at the current of whole devices at 1 A and 5 A is revealed in Figure 7. It is obvious that most of the magnetic field circulation is concentrated inside the structure as well as the distribution of the magnetic flux through the MRE railway pad is uniform. A slight magnetic field leakage is also found, while its value only reaches 0.27% to 1.45% on the MRE railway pad area. The magnetic flux density on the MRE railway pad increases with the enhancement of the coil current. The magnetic flux density on the MRE railway pad could be turned to 0.89 T by set the coil current to 5 A. Based on the simulation results, the designed structure of the electromagnetic device is capable to provide the desired magnetic flux density through the MRE railway pad as well as to minimizing the magnetic leakage.

3.3 Stiffness measurement

The static stiffness of the MRE railway pad is investigated by an electro-hydraulic-servo mechanical test system (322.25 load units,

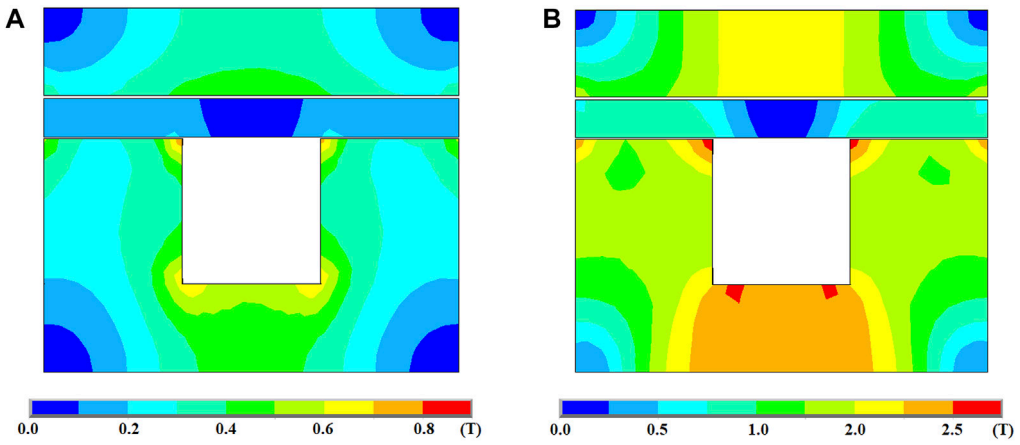

FIGURE 7
Magnetic field simulation of magnetic controlling unit coupled with MRE railway pad at 1A **(A)** and 5A **(B)**.

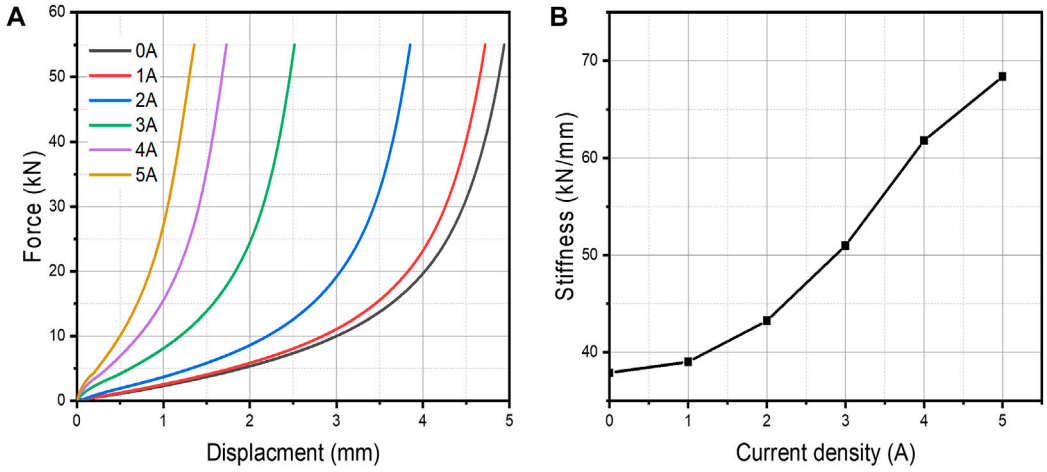

FIGURE 8
Load curve **(A)** and static stiffness **(B)** of MRE railway pad at different current on magnetic controlling unit.

MTS systems corporation). In the test procedure, the compressive load is applied at a rate of 60 kN/min from 0 kN to 55 kN three times, and holds for 1 min between every load loop. Six currents ranging from 0 A to 5 A are applied during the stiffness measurement. The third loading curve at different currents is illustrated in Figure 8A. It is obvious that the vertical displacement decreases with the enhancement of the applied magnetic field, resulting in the increasement of the static stiffness.

According to TB/T 3395.1-2015 standard (Fastening system for high-speed railway Part 1: General requirement), a clipping force is applied on the railway pads by rail clips after the fastening system is assembled. Therefore, the railway pad receives a preload (F_{pre}) of 20 kN without the train passing by. When the train passes through the fastening system, the train's loads are distributed to the railway pad *via* the rail (Knothe, K., et al., 2003). The average wheel weight ($F_{wheel\,load}$) of high-speed trains, for instance, is 70 kN with a load distribution coefficient (α) of 0.5 for a single fastening system, and at this moment the working load ($F_{working}$) of the railway pad is:

$$\boldsymbol{F_{working} = F_{pre} + \alpha \cdot F_{wheel\,load} = 55kN} \tag{6}$$

Therefore, the secant stiffness from 20 kN to 55 kN is commonly considered as the static stiffness of railway pad to evaluate the stiffness properties of railway pad, which can be represented by (Li, S., et al., 2020):

$$\boldsymbol{K_{static} = \frac{F_{55kN} - F_{20kN}}{D_{55kN} - D_{20kN}}} \tag{7}$$

Where $\boldsymbol{D_{55kN}}$ and $\boldsymbol{D_{20kN}}$ are the displacement measured under the force of 55 kN and 20 kN, in the third loading cycle, respectively. Figure 8B indicates that the static stiffness linearly enhances with the increasement of coil's currents. This is due to the MR effect on the MRE railway pad under the external magnetic field. Compared with the initial stiffness of 37.9 kN/mm without any external magnetic field, the maximum static stiffness of MRE railway pad reaches 68.4 kN/mm at 5 A, increasing by 80.5%. These results confirms that the tunable stiffness unit can change the stiffness properties of the railway fastening system. By further designing both the morphology of the MRE railway pad and structure of the whole unit, a more rational elastic pad which can sustain the heavy load with low stiffness can be developed.

3.4 Dynamic characteristics

The dynamic characteristics of the MRE railway pad are measured by a home-made instrument based on the single degree of freedom system as illustrated in Figure 9. The whole test system consists of an impact hammer, two bolts, two decoupling springs, an excitation block, several acceleration sensors, a concrete block and four spring vibration isolators. The MRE rail pad and magnetic controlling unit are placed underneath the center of the excitation block, the bolts are screwed up until the preload of excitation block reaches 20 kN to simulate fastened condition of the railway fastening system. During the measurement, an impact hammer with a Nylon head is used to stamp the center of the excitation block, which can acquire full resonance peak of excitation block within 1500 Hz. In the meanwhile, the excitation and acceleration signals are simultaneously recorded by a data signal-collecting device. The time-history curves of the excitation block after hammer stamped is illustrated in Figure 10A. By adding the coil's current in magnetic controlling unit, the peak value of acceleration response obviously descends with higher attenuation rates compared with zero current. This result indicates that the dynamic stiffness and damping properties of the MRE railway pad are increased by enhancing the coil's currents.

In order to extract the dynamic stiffness and damping constant, the frequency response curves are employed as shown in Figure 10B. The whole system can be simplified as the elastic and dashpot components of a mass-spring-damper single degree-of-freedom system in this condition (Zand, J. v. t. 1994; Kaewunruen, S. and Remennikov, A. 2021; Zhang, X., et al., 2020). In the vertical direction, the dynamic characteristics of the MRE railway pad can be described by a classic motion equation:

$$\boldsymbol{f(t) = m_p\ddot{x} + c_p\dot{x} + k_p x} \tag{8}$$

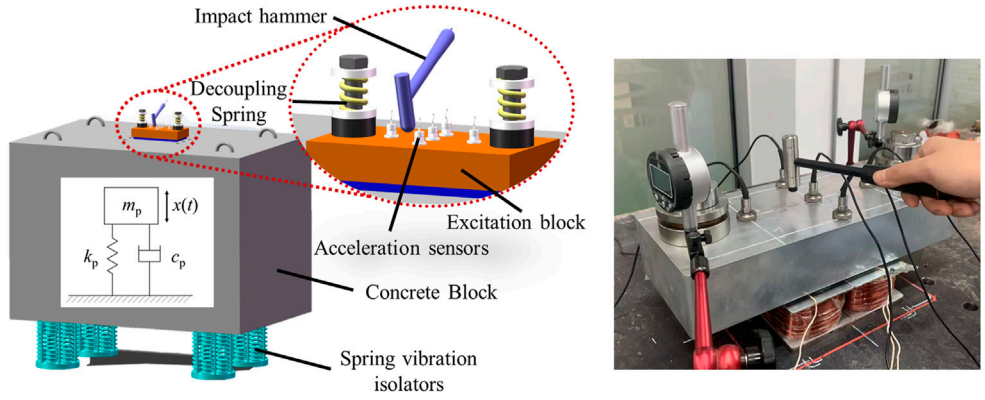

FIGURE 9
The experimental setup for characterizing the damping properties MRE railway pad with magnetic controlling unit.

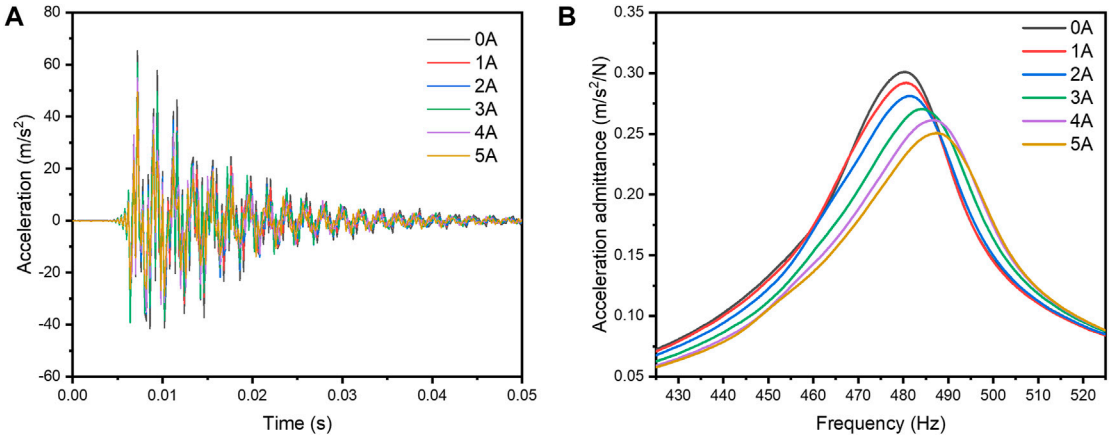

FIGURE 10
The acceleration **(A)** and frequency response function **(B)** of the MRE railway pad with different coil's currents.

where m_p, c_p, and k_p represent the effective mass, damping and stiffness of the MRE railway pad, respectively; $f(t)$ is the dynamic force on the single degree-of-freedom system; $\ddot{x}$, $\dot{x}$ and x are the displacement, speed and acceleration of the excitation block. In addition, the system resonance frequency (ω_n), damping ratio (ξ) and frequency ratio (r) can be described as:

$$\omega_n = \sqrt{\frac{k_p}{m_p}} \tag{9}$$

$$\xi = \frac{c_p}{2m_p\omega_n} \tag{10}$$

$$r = \frac{\omega}{\omega_n} \tag{11}$$

Thus, the frequency response function $\boldsymbol{H}(\omega)$ can be determined by taking the Fourier transformation of Eq. 8 and then the equation can be expressed as:

$$\boldsymbol{H}(\omega) = \frac{1}{m_p\omega_n^2}\frac{1}{\sqrt{(1-(r)^2)^2 + (2\xi r)^2}} \tag{12}$$

By substituting the Eqs 9–11 into the Eq. 11 and considering $\omega = 2\pi f$, then the magnitude of the frequency response function $\boldsymbol{H}(f)$ can be obtained as follows:

$$\boldsymbol{H}(f) = \frac{1}{m_p}\frac{4\pi^2\beta f^2}{\sqrt{\left[1-4\pi^2\beta f^2\right]^2 + \left[4\pi^2\beta\left(\frac{c_p^2}{k_p m_p}\right)f^2\right]}} \tag{13}$$

Where $\beta = \frac{m_p}{k_p}$.

It is obvious that the frequency response function $\boldsymbol{H}(f)$ is only determined by m_p, c_p, and k_p, which can be used as the curve-fitting parameters. The other parameters are obtained during the experimental process, in which the frequency response function $\boldsymbol{H}(f)$ can be calculated under the hammer impact. Hence, the dynamic stiffness and damping constant at resonance peak is obtained by the curve fitting results based on Eq. 13. In this equation, the dynamic stiffness is the sum stiffness of the railway pad and two decoupling springs, and therefore the dynamic stiffness of the MRE railway is the results after deducting the decoupling spring stiffness of 120.6 kN/mm, as

TABLE 3 The dynamic stiffness and damping properties of the MRE railway pad.

Coil's current (A)	Dynamic stiffness (kN/mm)	Damping constant (N·s/m)
0	354.4	8776.3
1	353.0	9097.7
2	353.8	9596.6
3	381.1	10036.3
4	392.1	10428.1
5	393.0	10866.3

shown in Table 3. The damping constant increases from 8776.3 N•s/m to 10866.3 N•s/m, and the dynamic stiffness increases from 354.4 kN/mm to 393.0 kN/mm, by changing the coil's current from 0 A to 5A. Compared with the MR efficiency of the MRE materials in DMA measurements, the percentage increase of dynamic stiffness and damping constant for the MRE railway pad is much lower, which may result from the higher baseline dynamic stiffness and the structures of the MRE railway pads.

4 Conclusion

In summary, an MRE railway pad is successfully designed and fabricated based on a thermal plastic silicone vulcanizate matrix, which can instead of the traditional railway pad in this work. The obtained MRE material indicates an obvious MR effect which can boost its storage modulus and loss factor under the magnetic field. The maximum MR efficiency of storage modulus and loss factor reaches 171% and 70%, respectively. According to the working conditions of the railway fastening system, the load of 55 kN can be applied on the railway pad for high-speed trains, the magnetic controlling unit is designed and porotype to deliver the magnetic field on the MRE railway pad. As suggested by the experimental results, the stiffness and damping properties of the MRE railway pad can be controlled by adjusting the coil's current. The static stiffness of the MRE railway pad exhibits an enhancement from 37.9 kN/mm to 68.4 kN/mm, and damping properties could increase from 8776.3 N•s/m to 10866.3 N•s/m, by adjusting the coil's current from 0 A to 5 A. These results successfully demonstrate an MRE railway pad with tunable stiffness and damping capability and pave the way for developing the MRE materials on more rational applications.

Data availability statement

The raw data supporting the conclusions of this article will be made available by the authors, without undue reservation.

Author contributions

SC and YW contributed conception and design of the whole study. YZ prepared the MRE samples. SC, YW, and CL developed the DMA clamps, the magnetic controlling unit and magnetic analysis. SC and BL tested the stiffness and damping properties of specimens. YW and JX supervised the research study and analyzed the experimental data. SC and YW wrote and edited the manuscript. All authors read, and approved the submitted version of manuscript.

Funding

This work was financially supported by the scientific research project of China Academy of Railway Sciences Co., Ltd. (2020YJ095), the National Natural Science Foundation of China (No. 52178441) and the scientific research project of China State Railway Group Co., Ltd. (N2021G050).

Conflict of interest

SC, BL, YW, and JX were employed by the company, Railway Engineering Research Institute, China Academy of Railway Sciences Group Co., Ltd.

BL, YZ, CL, YW, and JX were employed by the company, Beijing Tiekeshougang Railway Technology Co., Ltd.

The remaining authors declare that the research was conducted in the absence of any commercial or financial relationships that could be construed as a potential conflict of interest.

Publisher's note

All claims expressed in this article are solely those of the authors and do not necessarily represent those of their affiliated organizations, or those of the publisher, the editors and the reviewers. Any product that may be evaluated in this article, or claim that may be made by its manufacturer, is not guaranteed or endorsed by the publisher.

References

Ahmad Khairi, M. H., Mazlan, S. A., Choi, S., Abdul Aziz, S. A., Mohamad, N., et al. (2019). Role of additives in enhancing the rheological properties of magnetorheological solids: A review. *Advanced Engineering Materials* 21, 1800696. doi:10.1002/adem.201800696

Bastola, A. K., and Li, L. (2018). A new type of vibration isolator based on magnetorheological elastomer. *Materials & Design* 157, 431–436. doi:10.1016/j.matdes.2018.08.009

Behrooz, M., Wang, X., and Gordaninejad, F. (2014). Performance of a new magnetorheological elastomer isolation system. *Smart Materials and Structures* 23, 045014. doi:10.1088/0964-1726/23/4/045014

Chen, L., Gong, X.-L., Jiang, W.-Q., Yao, J. J., Deng, H. X., and Li, W. H. (2007). Investigation on magnetorheological elastomers based on natural rubber. *Journal of Materials Science* 42, 5483–5489. doi:10.1007/s10853-006-0975-x

Fu, J., Zheng, X., Yu, M., et al. "A new magnetorheological elastomer isolator in shear - compression mixed mode," in Proceedings of the IEEE/ASME International Conference on Advanced Intelligent Mechatronics, Wollongong, NSW, Australia, July 2013. doi:10.1109/AIM.2013.6584342

Gao, X., Wang, A., He, Y., and Gu, X. (2019). Structural improvement of the ω -type high-speed rail clip based on a study of its failure mechanism. *Shock and Vibration* 2019, 1–14. doi:10.1155/2019/4127065

Gong, X. L., Chen, L., and Li, J. F. (2007). Study of utilizable magnetorheological elastomers. *International Journal of Modern Physics B* 21, 4875–4882. doi:10.1142/s0217979207045785

Jvt, Z., Toward, M., Herron, D., Jones, C., et al. (1994). Assessment of dynamic characteristics of rail pads. *Rail Engineering International* 23.

Kaewunruen, S., and Remennikov, A. (2021). "Monitoring structural degradation of rail pads in laboratory using impact excitation technique," in *Faculty of Engineering* (Wollongong, Australia: University of Wollongong).

Khajehdezfuly, A. (2019). Effect of rail pad stiffness on the wheel/rail force intensity in a railway slab track with short-wave irregularity. *Proceedings of the Institution of Mechanical Engineers, Part F Journal of Rail and Rapid Transit* 233, 1038–1049. doi:10.1177/0954409718825410

Knothe, K., Yu, M., and Ilias, H. (2003). *Measurement and Modelling of Resilient Rubber Rail-Pads*. Berlin, Germany: Springer. doi:10.1007/978-3-540-45476-2_16

Li, S., Liang, Y., Li, Y., Li, J., and Zhou, Y. (2020b). Investigation of dynamic properties of isotropic and anisotropic magnetorheological elastomers with a hybrid magnet shear test rig. *Smart Materials and Structures* 29, 114001. doi:10.1088/1361-665x/ab9e09

Li, S., Watterson, P. A., Li, Y., Wen, Q., and Li, J. (2020). Improved magnetic circuit analysis of a laminated magnetorheological elastomer device featuring both permanent magnets and electromagnets. *Smart Materials and Structures* 29, 085054. doi:10.1088/1361-665X/ab8029

Li, W., Zhang, X., and Du, H. (2012). Development and simulation evaluation of a magnetorheological elastomer isolator for seat vibration control. *Journal of Intelligent Material Systems and Structures* 23, 1041–1048. doi:10.1177/1045389x11435431

Li, Y., Li, J., Li, W., and Samali, B. (2013). Development and characterization of a magnetorheological elastomer based adaptive seismic isolator. *Smart Materials and Structures* 22, 035005. doi:10.1088/0964-1726/22/3/035005

Li, Y., Li, J., Tian, T., and Li, W. (2013b). A highly adjustable magnetorheological elastomer base isolator for applications of real-time adaptive control. *Smart Materials and Structures* 22, 095020. doi:10.1088/0964-1726/22/9/095020

Liu, C., Hemmatian, M., Sedaghati, R., and Wen, G. (2020). Development and control of magnetorheological elastomer-based semi-active seat suspension isolator using adaptive neural network. *Frontiers in Materials* 7. doi:10.3389/fmats.2020.00171

Maes, J., Sol, H., and Guillaume, P. (2006). Measurements of the dynamic railpad properties. *Journal of Sound and Vibration* 293, 557–565. doi:10.1016/j.jsv.2005.08.042

Makarova, L. A., Alekhina, Y. A., Omelyanchik, A. S., Peddis, D., Spiridonov, V., Rodionova, V., et al. (2019). Magnetorheological foams for multiferroic applications. *Journal of Magnetism and Magnetic Materials* 485, 413–418. doi:10.1016/j.jmmm.2019.04.001

Moreno, M. A., Gonzalez-Rico, J., Lopez-Donaire, M. L., Arias, A., and Garcia-Gonzalez, D. (2021). New experimental insights into magneto-mechanical rate dependences of magnetorheological elastomers. *Composites Part B Engineering* 224, 109148. doi:10.1016/j.compositesb.2021.109148

Ph Papaelias, M., Roberts, C., and Davis, C. L. (2008). A review on non-destructive evaluation of rails: State-of-the-art and future development. *Proceedings of the Institution of Mechanical Engineers, Part F Journal of Rail and Rapid Transit* 222, 367–384. doi:10.1243/09544097JRRT209

Sainz-Aja, J. A., Carrascal, I. A., Ferreño, D., Pombo, J., Casado, J. A., and Diego, S. (2020). Influence of the operational conditions on static and dynamic stiffness of rail pads. *Mechanics of Materials* 148, 103505. doi:10.1016/j.mechmat.2020.103505

Schubert, G., and Harrison, P. (2015). Large-strain behaviour of magneto-rheological elastomers tested under uniaxial compression and tension, and pure shear deformations. *Polymer Testing* 42, 122–134. doi:10.1016/j.polymertesting.2015.01.008

Shuib, R. K., Pickering, K. L., and Mace, B. R. (2015). Dynamic properties of magnetorheological elastomers based on iron sand and natural rubber. *Journal of Applied Polymer Science* 132. doi:10.1002/app.41506

Sol-Sánchez, M., Moreno-Navarro, F., and Rubio-Gámez, M. C. (2015). The use of elastic elements in railway tracks: A state of the art review. *Construction and Building Materials* 75, 293–305. doi:10.1016/j.conbuildmat.2014.11.027

Sun, S., Yang, J., Du, H., and Li, W. (2017). Overcoming the conflict requirement between high-speed stability and curving trafficability of the train using an innovative magnetorheological elastomer rubber joint. *Journal of Intelligent Material Systems and Structures* 29, 214–222. doi:10.1177/1045389x17698591

Sun, S. S., Chen, Y., Yang, J., Tian, T. F., Deng, H. X., Li, W. H., et al. (2014). The development of an adaptive tuned magnetorheological elastomer absorber working in squeeze mode. *Smart Materials and Structures* 23, 075009. doi:10.1088/0964-1726/23/7/075009

Yasuhiro, U., Yusuke, Y., Kato, S., Kamoshita, S., Kawai, M., et al. (2018). Railway actuator made of magnetic elastomers and driven by a magnetic field. *Polymers* 10, 1351. doi:10.3390/polym10121351

Yoon, J-H., Lee, S-W., Bae, S-H., Kim, N. I., Yun, J. H., Jung, J. H., et al. (2022). Effect of cyclic shear fatigue under magnetic field on natural rubber composite as anisotropic magnetorheological elastomers. *Polymers* 14, 1927. doi:10.3390/polym14091927

Yu, Y., Li, J., Li, Y., Li, S., Li, H., and Wang, W. (2019). Comparative investigation of phenomenological modeling for hysteresis responses of magnetorheological elastomer devices. *Int J Mol Sci* 20, 3216. doi:10.3390/ijms20133216

Yu, Y., Royel, S., Li, J., Li, Y., and Ha, Q. (2016). Magnetorheological elastomer base isolator for earthquake response mitigation on building structures: Modeling and second-order sliding mode control. *Earthquakes and Structures* 11, 943–966. doi:10.12989/eas.2016.11.6.943

Yu, Y., Royel, S., Li, Y., Li, J., Yousefi, A. M., Gu, X., et al. (2020). Dynamic modelling and control of shear-mode rotational mr damper for mitigating hazard vibration of building structures. *Smart Materials and Structures* 29, 114006. doi:10.1088/1361-665X/abb573

Zhang, X., Thompson, D., Jeong, H., et al. (2020). Measurements of the high frequency dynamic stiffness of railway ballast and subgrade, *Journal of Sound and Vibration* 468, 115081. doi:10.1016/j.jsv.2019.115081